INSTYTUT FIZYKI JĄDROWEJ
INSTITUTE OF NUCLEAR PHYSICS
ИНСТИТУТ ЯДЕРНОЙ ФИЗИКИ

RAPORT No 1539/PL

FUSION – FISSION DYNAMICS

JAN BŁOCKI, JANUSZ BRZYCHCZYK
KAZIMIERZ GROTOWSKI, ROMAN PŁANETA

KRAKÓW 1991

FUSION - FISSION DYNAMICS

DYNAMIKA PROCESU FUZJA - ROZSZCZEPIENIE

Jan Błocki
Institute for Nuclear Studies, 05-400 Swierk, Poland
and
Roman Planeta, Janusz Brzychczyk, and Kazimierz Grotowski
Institute of Physics, Jagellonian University, Krakow, Poland
and
Institute of Nuclear Physics, Kraków, Poland

April 1991

WYDANO NAKŁADEM
INSTYTUTU FIZYKI JĄDROWEJ
IM. HENRYKA NIEWODNICZAŃSKIEGO
KRAKÓW, UL. RADZIKOWSKIEGO 152

Kopię kserograficzną, druk i oprawę wykonano w IFJ Kraków

Wydanie I *Zam. 49/91* *Nakład 90 egz.*

Abstract

Classical dynamical calculations of the heavy ion induced fission process for the reactions $^{40}Ar+^{141}Pr$, $^{20}Ne+^{165}Ho$ and $^{12}C+^{175}Lu$ leading to the iridium like nucleus have been performed. As a result prescission lifetimes were obtained and compared with the experimental values. The agreement between the calculated and experimental lifetimes indicates that the one-body dissipation picture is much more relevant in describing the Fusion-Fission dynamics than the two-body one. Somewhat bigger calculated times than the experimental ones in case of the C+Lu reaction at 16 MeV/nucleon may be a signal on the energy range applicability of the one-body dissipation model.

Streszczenie

Przeprowadzono obliczenia klasyczne dynamiki zderzeń ciężkich jonów prowadzące do rozszczepienia dla reakcji $^{40}Ar+^{141}Pr$, $^{20}Ne+^{165}Ho$ i $^{12}C+^{175}Lu$ prowadzących do irydopodobnego jądra złożonego. W wyniku uzyskano czasy życia do momentu rozerwania, które porównano z danymi eksperymentalnymi. Zgodność obliczonych i mierzonych czasów życia wskazuje że zastosowany model dyssypacji jednociałowej jest znacznie bardziej przydatny do opisu procesu typu Fusion-Fission niż dyssypacji dwuciałowej. W przypadku reakcji C+Lu przy energii 16 MeV/nukleon obliczone czasy życia są większe od wielkości eksperymentalnych co może wskazywać na zakres energetycznej stosowalności modelu jednociałowej dyssypacji.

1. Introduction

The dynamics of the heavy ion induced fission process is one of the most outstanding and still open questions in the nuclear physics. At least two fission scenarios are possible. The first one where an equilibrated compound system is formed, and the second one called usually fast fission [1]. The experimental investigation of such dynamics gives an excellent opportunity to test differant models of the energy dissipation. One of the models which is going to be tested in the present paper is the model of the so called one-body dissipation [2]. In this model it is assumed the motion of independent (noninteracting) nucleons colliding with the moving potential walls. In addition there is an exchange of particles between colliding ions giving rise to the so called window friction.

This model of dissipation was tested already in the calculations of the deep inelastic collisions of heavy ions at energies of the few MeV per nucleon giving a reasonable description as far as energy losses and angular distributions are concerned [3]. New experimental data of Zank et al [4] are now available on heavy ion induced fission dynamics. Three different reactions Ar+Pr at 7.9 MeV/A, Ne+Ho at 11 MeV/A and C+Lu at 16 MeV/A were investigated. All channels are leading to similar iridium like composite systems at moreless the same excitation energies. For these reactions by measuring pre and post-scission neutrons the transition times were deduced to be of the order of 10^{-20}sec - 10^{-19}sec.

As an outcome it was a conclusion that these long prescission lifetimes can not be explained by a two-body viscosity which at the same time provides a proper kinetic energy release in fission (Davies et al [5]). Zank et al hope that the observed discrepancy can probably be solved by assuming a mixture of a relative small two body and a large one body friction. It seems that before going to conclusion of taking a mixture of a two-body and one-body friction one should first check what are the results with the pure one-body friction. One can use here the coalescence and reseparation model [6]. It has been recently modified by including the charge degree of freedom and the temperature feedback [7,8].

The outline of this paper can be summarized in the following words. In Sec.2 the idea of the calculations is briefly described, in Sec.3 results of the calculations and their comparison with the experiment are presented and in Sec.4 there are final remarks and conclusions.

2. Idea of the calculations

The idea of the calculations is the following: the system of the classical dynamical Rayleigh-Lagrange equations of motion is solved numericaly following the dynamical trajectory of colliding ions from the point they start to interact till they reseparate (scission) again. Let us now describe briefly the parametrization of nuclear shapes and the main terms entering equations of motion.

2.1. Parametrization of nuclear shapes

Nuclear shapes are considered to be axialy symmetric consisted of two spheres connected smoothly by a quadratic portion of the surface of revolution (Fig.1). In Fig.1a) there is an example of the prescission shapes and in Fig.1b) of the postscission shapes. Parameters (ρ,λ,Δ) defined in Fig.1 describe fully the volume conserved shapes.

In addition to the macroscopic variables (ρ,λ,Δ) there are three rotational degrees of freedom (ϕ_1,ϕ_2,ϕ) and three angular velocities $(\omega_1,\omega_2,\omega)$ connected with the rotation of sphere 1 and sphere 2 and the rotation of the shape as a whole. Altogether there are six independent variables and corresponding six coupled equations of motion.

2.2. Potential energy

The potential energy of the shape under the question is calculated as a sum of the nuclear part and the Coulomb part. The nuclear part using a double folding procedure developed by Krappe,Nix and Sierk [9] can be written as:

$$V_n = -\frac{C_s}{8\pi^2 r_0^2 a^3}\iint \left(\frac{\sigma}{a}-2\right)\exp(-\sigma/a)/\sigma \; d_3r \; d_3r' \qquad (1)$$

where $\sigma = |\vec{r}-\vec{r}'|$, $C_s = a_s(1-\kappa_s I^2)$ and $I=(N-Z)/A$. Parameters r_o, a, a_s and κ_s were taken from the fit done by Krappe et al [9] in their original peper. For axialy symmetric shapes the expression (1) reduces to the three dimensional integral of the following type:

$$V_n = \frac{C_s}{4\pi r_o^2} \iiint \{2-[(\sigma/a)^2+2(\sigma/a)+2]\exp(-\sigma/a)\}\cdot$$

$$P(z)[P(z)-P(z')\cos\phi - \frac{dP}{dz}(z-z')]\cdot \qquad (2)$$

$$P(z')[P(z')-P(z)\cos\phi - \frac{dP}{dz'}(z'-z)]\, dz\, dz'\, d\phi/\sigma^4$$

where $\tilde{\rho}=P(z)$ is the equation of the nuclear surface in cylindrical coordinates $(\tilde{\rho}, z, \phi)$. One has to be careful in evaluating expression (2) as factors C_s in front of the integral depend on the isospin $I=(N-Z)/A$ which is different on both sides of the nucleus. First one has to establish how to split the shape (like the one in Fig.1a) into two parts with charge numbers Z_1 and Z_2. It was decided that the border line splits the shape into two parts whose volumes are in the ratio of two masses A_1/A_2. As the integral in the expression (2) is over the surface of the shape one has to integrate not only over the outer surface but also along this border line which would not be the case if the charge distribution would be uniform everywhere. Calculating the integral in the expression (2) the shape was split into four parts: the sphere 1, the neck from the matching point with sphere 1 to the border line, the neck from the border line to the matching point with sphere 2 and the sphere 2. In each part the eight points Gauss method was used in numerical evaluation of integral (2).

The similar procedure has to be done in calculating the Coulomb part of the potential which for axialy symmetric shape can be written as:

$$V_c = \frac{\pi}{3}\rho_z\rho_{z'}\iiint \{P(z)P(z')(P(z)-P(z')\cos\phi - \frac{dP}{dz}(z-z'))\cdot$$

$$(P(z')-P(z)\cos\phi - \frac{dP}{dz'}(z'-z))\}/ \qquad (3)$$

$$(P(z)^2+P(z')^2-2P(z)P(z')\cos\phi+(z-z')^2)^{1/2}\, dz\, dz'\, d\phi$$

where ρ_z and $\rho_{z'}$ are the charge densities.

One should also remember that having two different isospins on both sides of the nucleus one has to split the volume part of the energy $E_V = a_v(1-\kappa_v I^2)A$ into two parts changing in time. Finally the total potential energy will be

$$V_{tot} = V_N + V_C + E_V \qquad (4)$$

2.3. Kinetic Energy

It is assumed that the collective kinetic energy of the shape variables (ρ,λ,Δ) is of the quadratic form calculated from the irrotational mass flow in the Werner - Wheeler approximation [10]

$$T = \frac{1}{2} \sum_{i,j} M_{i,j} \dot{q}_i \dot{q}_j \qquad (q_i=\rho,\lambda,\Delta) \qquad (5)$$

The matrix element $M_{\rho\rho}$ of the mass tensor was checked for two separated spheres being exactly the reduced mass.

In the rotational degrees of freedom kinetic energy is equal to:

$$T_r = \frac{1}{2} I_{rel} \omega^2 + \frac{1}{2} I_1 \omega_1^2 + \frac{1}{2} I_2 \omega_2^2 \qquad (6)$$

where I_1 and I_2 are rigid moments of inertia of sphere 1 and 2, respectively and $I_{rel}=I_{tot}-I_1-I_2$ where I_{tot} is the rigid moment of inertia of the whole nucleus. Two spheres can rotate independently from the relative rotation but due to the tangential friction after some time all the frequencies ω, ω_1 and ω_2 are moreless equal and the body rotates as a rigid one.

In Fig.2 the dependence of the angular velocities of fragments ω_1 and ω_2 and the relative one ω as a function of time for Ar+Pr reaction at the initial angular momentum L=100h is shown. At the beginning fragments (spheres) do not rotate ($\omega_1=\omega_2=0$) and there is only a relative rotation. After some time fragments due to the tangential friction start to rotate and overall rotation of the system as a whole slows down as the moment of inertia is increasing due to the elongation. After a time of about $1.2\cdot10^{-21}$sec all three angular velocities ω, ω_1 and ω_2 become moreless the same and from that point on the system rotates as a rigid.

2.4. One-body Dissipation

The mechanism of the energy dissipation adopted is of the one-body type [2] which means the dissipation arises due to collisions of independent particles with walls of the moving nucleus. There are two limiting cases in which two different simple formulas for the rate of the dissipated energy can be derived. The first one is so called the mononuclear regime when the system of colliding ions can be considered as a monosystem with a thick neck. In that case the gas of nucleons can be considered as a relaxed Fermi gas and the rate of the energy dissipation is given by the following wall formula:

$$\left(\frac{dE}{dt}\right)_{wall} = \rho_m \bar{v} \oint dS(\dot{n}-D)^2 \qquad (7)$$

where ρ_m is the mass density of nucleons, $\bar{v}$ is the average speed of nucleons (equal to three quarters of the Fermi velocity in the Fermi gas model), dS is the element of nuclear surface, $\dot{n}$ is the normal velocity of walls and D is the overall drift velocity of the gas of nucleons ensuring the invariance of the formula (7) against translations and rotations.

In the second limiting case called the dinuclear regime when two ions are either separated or connected by a thin neck the formula (7) can not be applied as we are dealing with two Fermi gases separated by the collective velocity. In that case the so called wall plus window formula can be applied and it reads as follows:

$$\left(\frac{dE}{dt}\right)_{w+w} = \rho_m \bar{v} \int dS(\dot{n}-D_1)^2 + \rho_m \bar{v} \int dS(\dot{n}-D_2)^2$$
$$+\frac{1}{4}\rho_m \bar{v} S_w(u_t^2+2u_r^2) + \frac{16}{9}\frac{\rho_m \bar{v}}{S_w}\dot{V}_1^2 \qquad (8)$$

The first two terms correspond to the wall formula (eq.7) but are calculated for each fragment separately with drifts D_1 and D_2 for each of the gases. The third term is associated with the dissipation due to the exchange of particles through the window of the area S_w. Components of the relative velocity of two fragments u_t and u_r correspond to the velocities parallel and perpendicular to the window. The last term in eq.8 corresponds to the dissipative resistance against the asymmetry changes [11] with $\dot{V}_1$ being the rate of the change of the volume of fragment 1. Equations 7 and 8 express the rate of the dissipated energy in two limiting cases called mononuclear and dinuclear regimes. In general when the situation is in between these two limiting cases a smooth transition between formulas 7 and 8 is used [8]:

$$\frac{dE}{dt} = f\left(\frac{dE}{dt}\right)_{wall} + (1-f)\left(\frac{dE}{dt}\right)_{w+w} \qquad (9)$$

with a form factor f going to 1 for sphere or spheroid like shapes and going to 0 at scission.

2.5 Equations of motion

The system of the classical Rayleigh - Lagrange equations to be solved can be written in the form:

$$\frac{d}{dt}\frac{\partial L}{\partial \dot{q}_i} + \frac{\partial \Phi}{\partial \dot{q}_i} = \frac{\partial L}{\partial q_i} \qquad (10)$$

with L=T-V being a Lagrangian which is the difference of the kinetic and potential energies and Φ being half the rate of the dissipated energy. Quantities q_i form a set of the macroscopic and angular variables $q_i = (\rho, \lambda, \Delta, \theta, \theta_1, \theta_2)$. So altogether there are six second order differential equations to be solved. In addition there are two other equations. One of them for the time derivative of the difference in the excitation energies of both parts of the nuclear system

$$\frac{d(E_1^* - E_2^*)}{dt} = \left(\frac{dE}{dt}\right)^1_{wall} - \left(\frac{dE}{dt}\right)^2_{wall} + 2T_0\dot{S}_{21} \qquad (11)$$

where first two terms are defined in Section 2.4 and the last one is due to the temperature feedback with $T_0=\frac{1}{2}\cdot(T_1+T_2)$ being an average temperature of the T_1 and T_2, the temperatures of the first and the second fragment, respectively. $\dot{S}_{21}$ is the entropy flux taken from Feldmeier [3].

For asymmetric collisions the particle exchange between two fragments leads to the temperature mismatch which means that the smaller fragment becomes hotter than the bigger one. This gives an extra flux of particles from the smaller to the bigger fragment. This effect works efficiently in the early stage of the collision but after some time when temperatures become moreless equal it disappears. In Fig.3 temperatures of the projectile like fragment and target like fragment for three reactions under investigation: $^{41}Ar + ^{141}Pr$ at L=100$\hbar$, $^{20}Ne + ^{165}Ho$ at L=90$\hbar$ and $^{12}C + ^{175}Lu$ at L=80$\hbar$ are presented. The three upper curves correspond to the projectile like fragments and the three lower ones to the target like fragments. As one can see the temperature of the target like fragments goes monotonicaly up and moreless in the same way for all three targets. At the same time the temperature of the corresponding projectiles goes up at the beginning much faster than the temperature of targets and reaches its maximum at the time around $0.3 - 0.4 \cdot 10^{-21}$sec. After that the temperature feedback mechanism is cooling down the

projectile like fragment bringing both partners to the temperature equilibrium after the time of about $1.3 \cdot 10^{-21}$sec. Maximas of the projectile like fragment curves are different for different projectiles showing the highest value for the smallest C nucleus and the lowest for the Ar. This reflects the fact that moreless the same in all cases exchange of particles leads to the bigger temperature for the lighter nucleus.

Another equation is for the time derivative of one of the charges, let say Z_1:

$$\frac{dZ_1}{dt} = fl_2 \frac{Z_2}{A_2} - fl_1 \frac{Z_1}{A_1} \qquad (12)$$

where fl_1 is the flux of all the particles (neutrons and protons) through the window from the vessel 1 to the vessel 2 and fl_2 is the same in the opposite direction. Z_1, A_1 and Z_2, A_2 are charges and masses of the part 1 and 2.

In Fig.4 the ratio Z/A as a function of time for three reactions investigated is shown. In all cases the charge equilibration takes place in the time which is shorter than $1 \cdot 10^{-21}$sec. and afterwards the charge is uniformly distributed over the whole shape. Besides this time for the charge equilibration is moreless the same in all the cases which is supported by the experimental results of Planeta et al [12].

Equations (10),(11) and (12) are solved numericaly by the predictor-corrector method. At the same time conservation laws it means the energy and angular momentum conservations are checked being all the time on the level of accuracy less then 0.1%.

3. Results

Typical model trajectories are presented in Fig.5 for the Ne + Ho case. Angular momentum of each trajectory is indicated. The L=105h trajectory is characterized by a small total mass transfer from the target to the projectile of only one mass unit. The transition time of this trajectory is $0.95 \cdot 10^{-21}$sec. Such trajectory is a typical case for a Deep Inelastic Collision (DIC) where identity of the interacting fragments is preserved. The next L=75h trajectory stops at the point ρ=0.93, λ=1.31, Δ=0 where the effective potential $V_{eff}=V_N+V_C+V_R$ has a local minimum. This can be understood as a compound nucleus formation. The most interesting for reactions studied in the present paper is the

L=90ħ trajectory. Here the total mass transfer is 57.25 mass units and the corresponding transition time is $44.7 \cdot 10^{-21}$sec (6 revolutions of the system).

Transition between different reaction regimes is well illustrated by the percentage of the possible mass drift vs angular momentum (see Fig.6). Two of the reactions in question, C+Lu and Ne+Ho are characterized by a well defined border between the DIC and the Fusion-Fission region. Particularly exotic is the C+Lu case where a decrease of angular momentum from 85ħ to 84ħ gives an increase of the mass transfer of 75 mass units. For Ar+Pr a gradual increase of mass transfer is observed as a function of angular momentum.

In calculations one has to decide what is the L window for Fusion - Fission processes. It was decided to take the upper limit of the L value at which there are more than 10 nucleons transferred from target to the projectile. Above this L value there is a typical picture of the Deep Inelastic Collision in which target and projectile do not loose their identity. This criterion for establishing the upper limit of the L value is not so important for $^{20}Ne+^{165}Ho$ and $^{12}C+^{175}Lu$ reactions where the distinction between Fusion - Fission and Deep Inelastic Collision is clearly visible and very sharp. It is much more important for the $^{40}Ar+^{141}Pr$ reaction where transfer of nucleons from target to projectile goes smoothly with the incoming L and depending where the border is the final results can be slightly different. The upper value of L is however not very important in calculating average transient times as at these L values times are short not contributing too much to the average.

The lower limit of the L value was taken below which the system fuses and does not want to reseparate any more. This corresponds to the region where experimentally the evaporation residues are observed. Established in these ways L windows for the Fusion - Fission processes are somewhat different from the experimental ones and shifted towards higher L values.

In Fig.7 three dynamical trajectories in the (ρ,λ) plane for reactions $^{12}C+^{175}Lu$ at L=80ħ, $^{20}Ne+^{165}Ho$ at L=90ħ and $^{40}Ar+^{141}Pr$ at L=100ħ are presented. The values selected for the angular momenta are placed inside of the Fusion-Fission windows. On top of the trajectories the corresponding nuclear shapes are shown. As one can see at the beginning of the trajectory or close to it the shape is very much asymmetric with the asymmetry corresponding to the initial one of two colliding nuclei. At the end when trajectories are close to the scission

(broken) line in all the cases shapes become symmetric or almost symmetric in all the cases. One should keep in mind that in Fig.7 only the projection of the trajectories in the (ρ,λ) plane is presented. In reality those trajectories should be seen in the three dimensional space (ρ,λ,Δ).

In Fig.8 the trajectory for the reaction $^{20}Ne + ^{165}Ho$ at L=90h at three different cuts of the potential at Δ = 0.32879, 0.24612 and 0.12874 is shown. The potential in Fig.8 is the sum of the static part and rotational energy, where rotation is treated as a rigid one. This last assumption is justified from the early stage of the collision (see Fig.2) and gives the real impression of what kind of the potential the nuclear system is feeling most of the time. In the uppermost part of Fig.8 the potential for the initial asymmetry Δ=0.32879 is drawn. The point at the trajectory corresponding to this asymmetry is shown by the cross. At the beginning the trajectory goes up the potential having still some of the initial kinetic energy. Later on it goes down the potential very slowly with almost no kinetic energy. If the asymmetry would not change the trajectory would continue to go up the picture but due to the asymmetry changes the potential landscape varies dramaticaly (the lower part of Fig.8) and the trajectory makes a turn toward lower potential value. Now the potential is driving the system towards the reseparation (scission line) and due to the flatness of it the system is moving very slowly giving at the end long transient times.

In Table I summary of the results of the calculations together with the experimental results are presented. For comparison with transition times measured by Zank et al [13] the corresponding values of time τ averaged over the Fusion-Fission L window were calculated.

Table I

reaction	E_{LAB}(MeV)/A	Experiment $L_{win}(\hbar)$	Experiment $\tau(10^{-21}s)$	Calculations $L_{win}(\hbar)$	Calculations $\tau(10^{-21}s)$
Ar + Pr	7.9	50-109	14^{+35}_{-8}	100-130	13.3
Ne + Ho	11	57-94	60^{+45}_{-25}	77-100	72.3
C + Lu	16	49-62	40^{+15}_{-15}	79-84	112.4

For the first two reactions in Table I the agreement of the calculated average τ value with the experimental τ is excellent whereas for the reaction Lu+C the calculated time is much bigger than the experimental value. One should keep in mind that the experimental errors are in all cases rather big, however in the Lu+C case the calculated value is outside these error limits. For angular momentum windows the second reaction displays a fair agreement between the measured and calculated values. The agreement is worse for the first reaction and quite unsatisfactory for the last one.

4. Discussion and Conclusions

Calculations presented here describe three Heavy Ion Reactions resulting in nearly symmetric splitting of iridium like composite systems. Although they do not proceed via the classical compound nucleus formation their fairly long prescission times (the composite system makes up to 40 revolutions before scission) allow to enlist them to the Fusion-Fission class. To obtain such a long prescission times in the two-body friction picture one would have to increase the two-body viscosity coefficient by a factor of 7 compared to the one determined by Davies et al [10]. One could therefore say that the one-body dissipation picture employed in these calculations is much more relevant in describing the Fusion - Fission dynamics than the two-body one.

In experiments of Zank et al the Compound Nucleus-Fission mechanism could not been distinguished from this which is called here the Fusion-Fission one. This can be partly responsible for some L window disagreements. The comparison with the experiment presented in Table I

shows that calculated times for the Lu+C reaction are somewhat bigger than the experimental ones. One of the possible explanations is that for the carbon projectile at the energy 16 MeV per nucleon there is quite a significant part of the incomplete fusion processes in the experiment which can efficiently shadow the experimental result. Independently on the incomplete fusion contribution the disagreement could be in this case a signal on the energy range applicability of the one-body dissipation model. One could imagine that at 16 MeV per nucleon incident energy the Pauli principle does not work so efficiently and there are at least in the first stage of the collision a lot of the two-body correlations which can affect the whole dynamics of the process significantly. Nevertheless below the energy mentioned (16 MeV per nucleon) nice agreement between experiment and calculations indicates for the one-body mechanism of dissipation as a proper one contrary to the two-body mechanism.

References

1. M.F.Rivet, R.Alami, B.Borderie, H.Fuchs, D.Gardes and H.Gauvin
   Z.Phys.A330,295(1988)
   H.Keller, K.Lutzenkirchen, J.V.Kratz, G.Wirth, W.Bruchle and K.Summerer
   Z.Phys.A328,313(1987)
   W.Q.Shen, J.Albinski, A.Gobbi, S.Gralla, K.D.Hildenbrand, N.Herrmann, J.Kuzminski, W.F.J.Muller, H.Stelzer, J.Toke, B.B.Back, S.Bjornholm and S.P.Sorensen.
   Phys.Rev.C36,115(1987)
2. J.Blocki, Y.Boneh, J.R.Nix, J.Randrup, M.Robel, A.J.Sierk and W.J.Swiatecki
   Ann.Phys.113,330(1978)
3. J.Blocki, M.Dworzecka, F.Beck and H.Feldmeier
   Phys.Lett.99B,13(1981)
   H.Feldmeier
   reprint ANL-PHY-85-2(1985)
4. W.P.Zank, D.Hilscher, G.Ingold, U.Jahnke, M.Lehmann and H.Rosner
   Proc. Intl School Seminar on Heavy Ion Physics, Dubna 1989
   Phys.Rev.C33,519(1986)
5. K.T.R.Davies, A.J.Sierk and J.R.Nix
   Phys.Rev.C13,2385(1976)
6. J.Blocki, H.Feldmeier and W.J.Swiatecki
   Nucl.Phys.A459,145(1986)
7. J.Blocki, K.Grotowski and R.Planeta
   Proc. Intl School Seminar on Heavy Ion Physics, Dubna 1989
8. L.G.Moretto, Z.Physik A310,61(1983)
9. H.Krappe, J.R.Nix and A.J.Sierk
   Phys.Rev.C20,992(1979)
10. I.Kelson, Phys.Rev.136,B1667(1964)
11. J.Randrup and W.J.Swiatecki, Nucl.Phys.A429,105(1984)
12. R.Planeta, S.H.Zhou, K.Kwiatkowski, W.G.Wilson, V.E.Viola, H.Breuer, D.Benton, F.Khazaie, R.J.McDonald, A.C.Migneerey, A.Weston-Dawkes, R.T.deSouza, J.H.Hulzenga, W.U.Schroder, Phys.Rev.C38,195(1988)
13. D.Hilscher, D.J.Hinde and H.Rossner
    preprint HMI-P 87/15 R

Figure Captions

1. Parametrization of the nuclear shape. a)-prescission shape and b)-postscission shape.
2. The time dependence of the angular velocities of fragments ω_1 and ω_2 and the relative one ω for the reaction Ar+Pr at L=100ħ.
3. The dependence of the temperatures of projectile (three upper curves) and target (three lower curves) like fragments on time. The solid line corresponds to the reaction C+Lu at L=80ħ, the broken one to Ne+Ho at L=90ħ and the dot-dashed one to Ar+Pr at L=100ħ.
4. The dependence of the Z/A of projectile (three upper curves) and target (three lower curves) like fragments on time. The three cases are the same as in Fig.3.
5. Three typical trajectories for the reaction Ne+Ho at L=75ħ, 90ħ and 105ħ in (ρ,λ) plane. The scission line is indicated by the solid line.
6. The percentage of the possible mass drift vs angular momentum L for three reactions indicated.
7. Dynamical trajectories in (ρ,λ) plane for C+Lu at L=80ħ, Ne+Ho at L=90ħ and Ar+Pr at L=100ħ. The corresponding nuclear shapes along trajectories are shown.
8. The trajectory (broken line) for the reaction Ne+Ho at L=90ħ at three different cuts of the potential at Δ=0.32879, 0.24612 and 0.12874. Points along trajectories corresponding to these asymmetries Δ are indicated by crosses. The dotted line indicates the scission line.

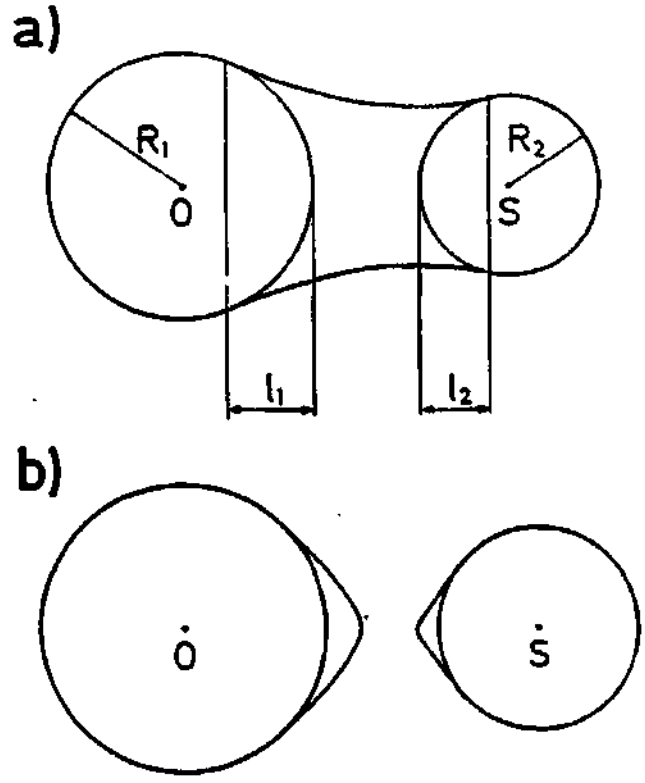

$$\rho = \frac{S}{R_1 + R_2}$$

$$\lambda = \frac{l_1 + l_2}{R_1 + R_2}$$

$$\Delta = \frac{R_1 - R_2}{R_1 + R_2}$$

Fig.1

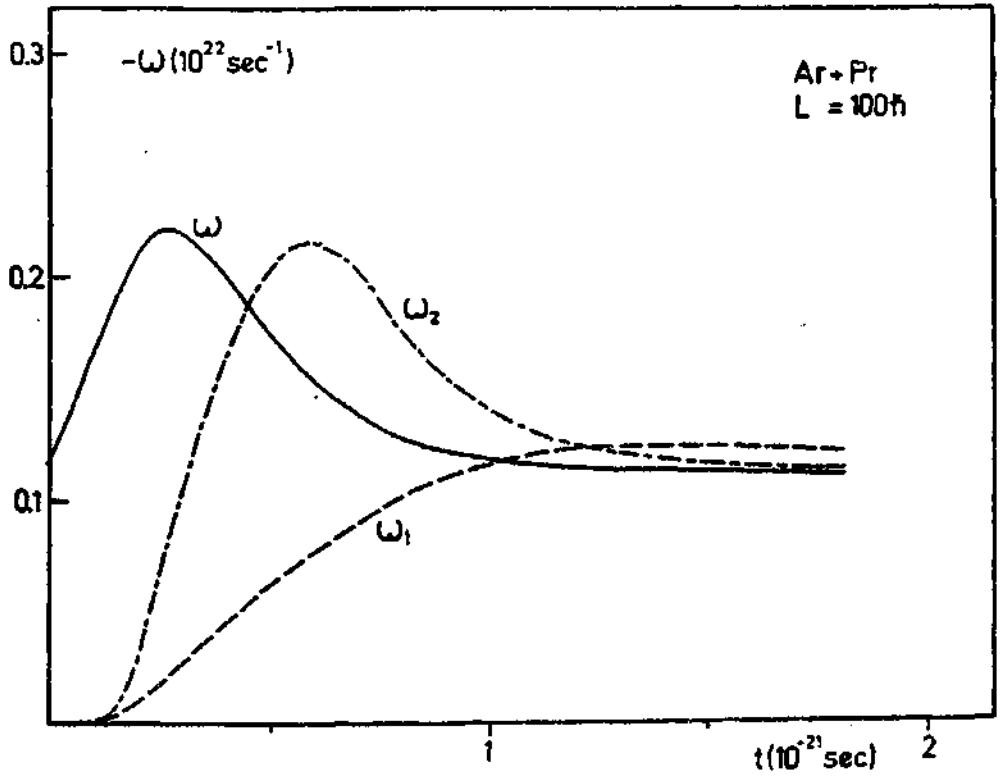
0.3
0.2
0.1
$-\omega(10^{22}sec^{-1})$
Ar+Pr
L = 100 Å
ω
ω_2
ω_1
1
2
$t(10^{-21}sec)$

Fig.2

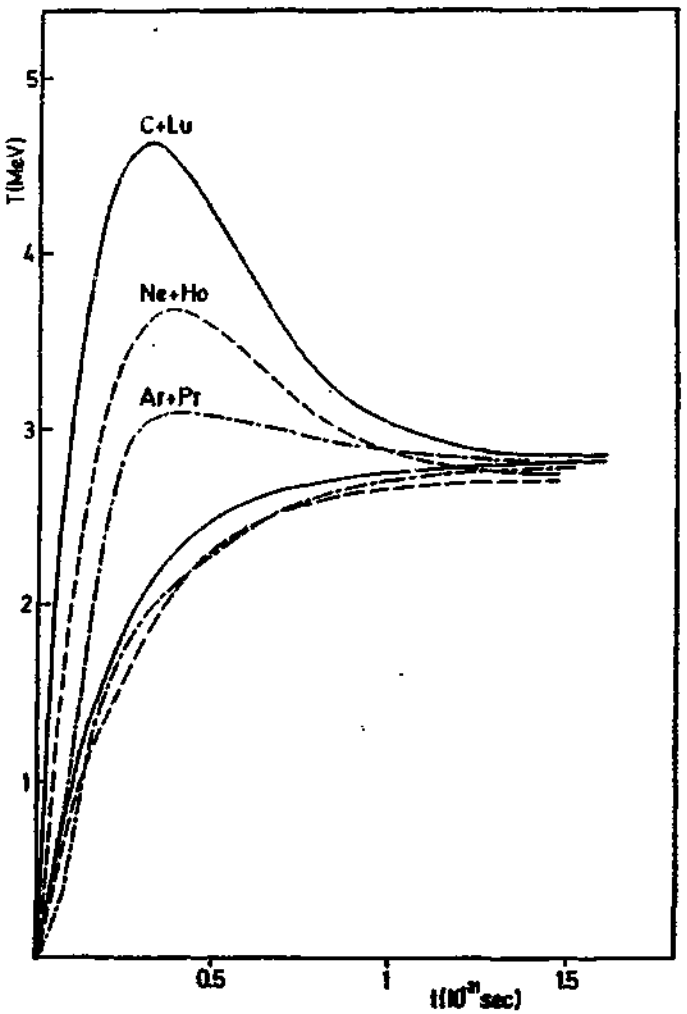

Fig.3

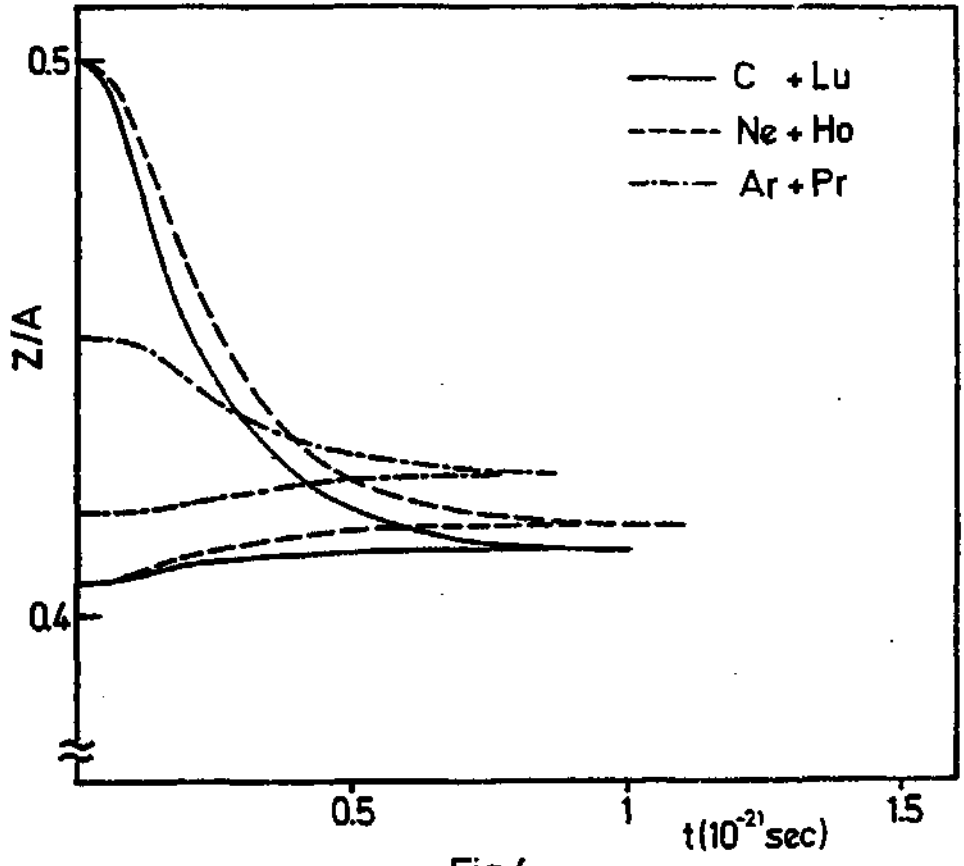

Fig.4

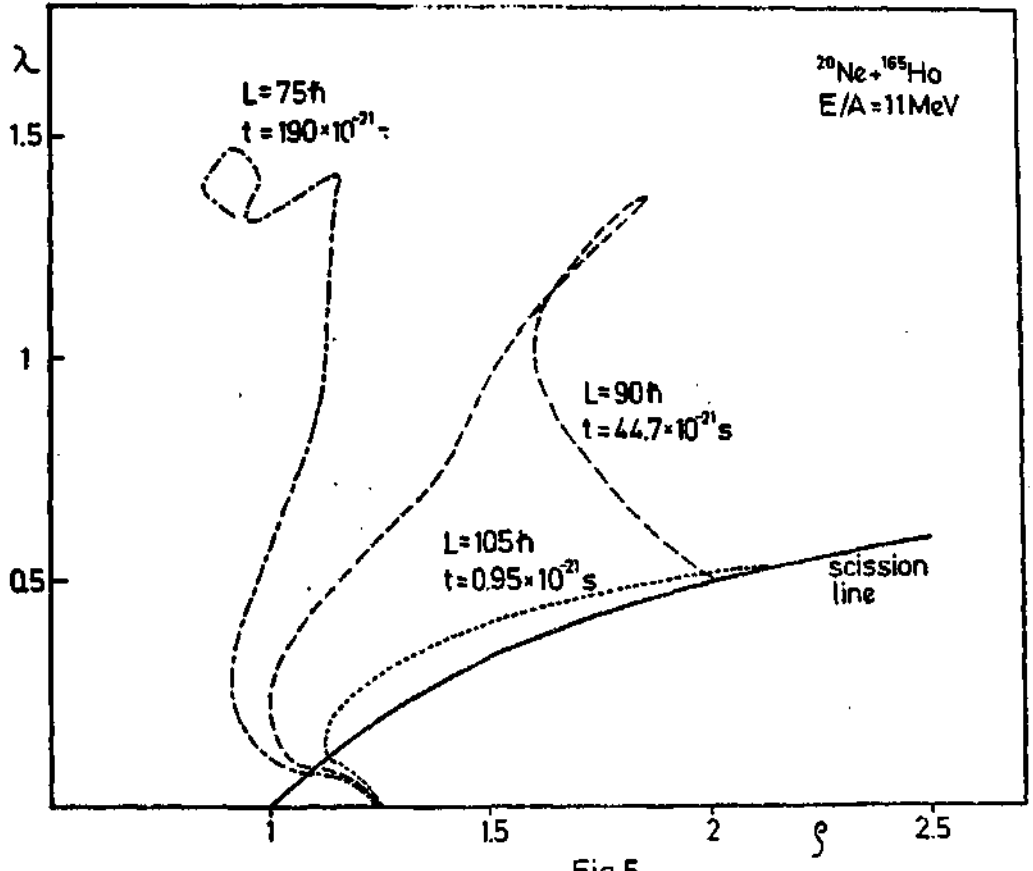
λ
1.5
1
0.5
1
1.5
2
ρ
2.5
L=75ħ
t=190×10⁻²¹s
L=90ħ
t=44.7×10⁻²¹s
L=105ħ
t=0.95×10⁻²¹s
scission line
²⁰Ne+¹⁶⁵Ho
E/A=11MeV

Fig.5

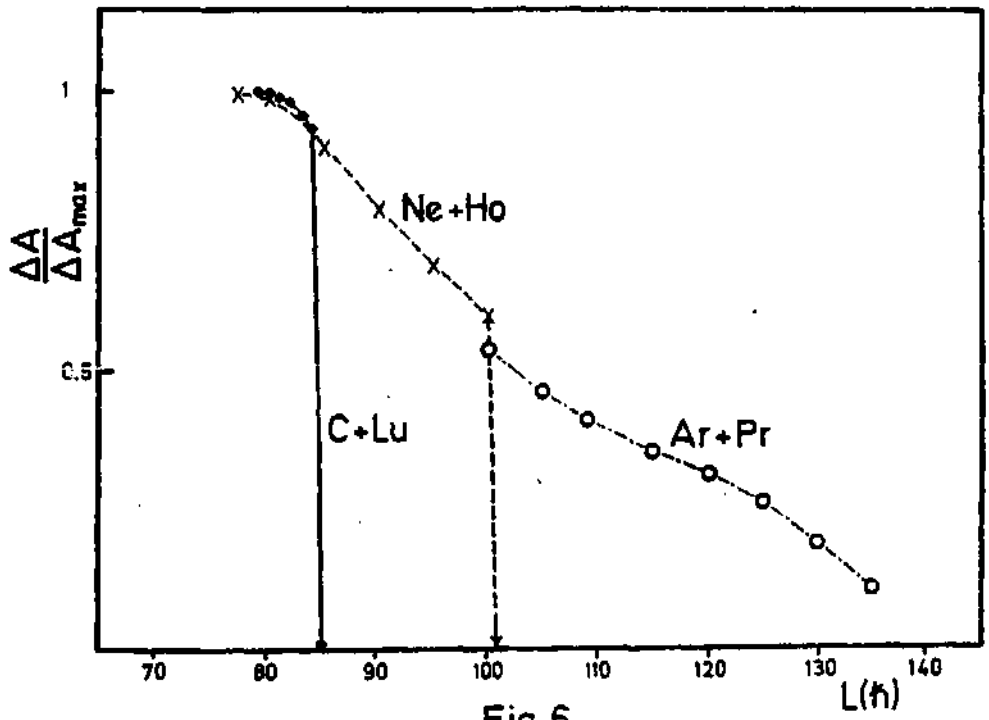
1
0.5
$\frac{\Delta A}{\Delta A_{max}}$
Ne+Ho
C+Lu
Ar+Pr
70
80
90
100
110
120
130
140
L(ħ)

Fig.6

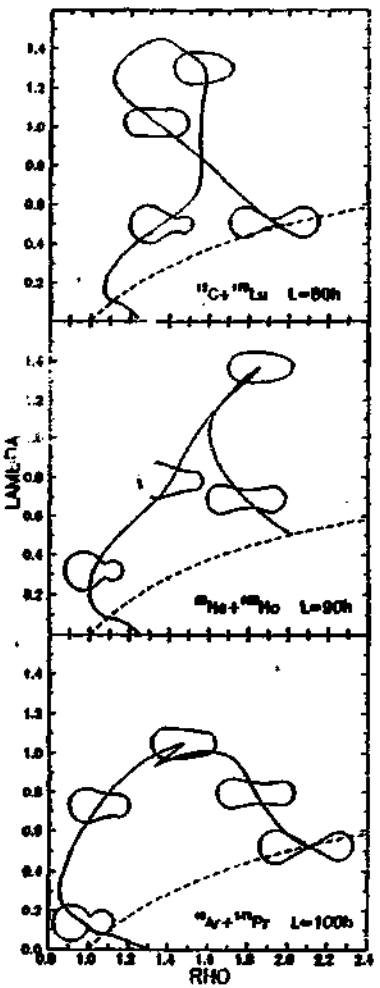

Fig.7

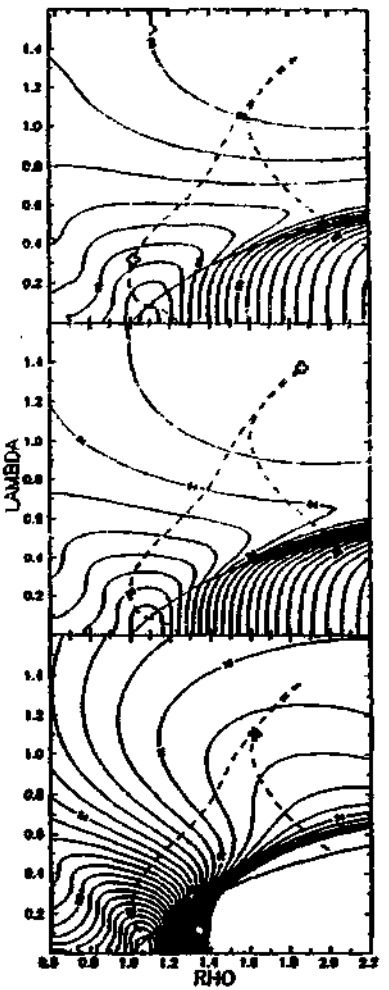

Fig.8